Low symmetry aspects inherent in EMR studies of the orthorhombic to monoclinic structural phase transition in the hexagonal form of barium titanate $BaTiO_3$ doped by Fe^{3+} ions

2008 J. Phys.: Condens. Matter 20 295219

(http://iopscience.iop.org/0953-8984/20/29/295219)

J. Phys.: Condens. Matter **20** (2008) 295219 (13pp) doi:10.1088/0953-8984/20/29/295219

Low symmetry aspects inherent in EMR studies of the orthorhombic to monoclinic structural phase transition in the hexagonal form of barium titanate $BaTiO_3$ doped by Fe^{3+} ions

C Rudowicz[1], **P Gnutek and P Budzyński**

Modeling in Spectroscopy Group, Institute of Physics, Szczecin University of Technology, Aleja Piastów 17, 70-310 Szczecin, Poland

E-mail: crudowicz@ps.pl

Received 2 May 2008, in final form 10 June 2008
Published 1 July 2008
Online at stacks.iop.org/JPhysCM/20/295219

Abstract

Electron magnetic resonance (EMR) studies reveal different spectroscopic properties of transition ions doped in the two crystallographically different forms of barium titanate: cubic (normal) c-$BaTiO_3$ and hexagonal polymorph h-$BaTiO_3$. Recent comparative analysis of EMR data helped to solve the controversy concerning the disparate zero-field splitting (ZFS) parameters for Fe^{3+} ions in c-$BaTiO_3$. This paper deals with the low symmetry aspects inherent in EMR studies of the orthorhombic to monoclinic structural phase transition in h-$BaTiO_3$ doped by Fe^{3+} ions. Pertinent spin Hamiltonian notations and choices of axis systems are clarified. The second- and fourth-rank ZFS parameters determined by EMR and the second-rank ones computed using a superposition model for the Fe^{3+} ions in h-$BaTiO_3$ are reanalyzed. The available ZFS parameters are presented in a well-defined axis system and in a unified way to ensure meaningful comparison. Pertinent transformations of ZFS parameters are carried out using the package CST. Simulations of the low symmetry ZFS parameters are carried out to assess the role of monoclinic and triclinic ZFS terms and to investigate the low symmetry aspects arising with lowering of temperature during the orthorhombic to monoclinic structural phase transition in Fe^{3+}:h-$BaTiO_3$. The procedure for analyzing experimental and theoretical ZFS parameters for transition ions at monoclinic and triclinic symmetry sites proposed here enables a better understanding of the low symmetry aspects involved. This study suggests the need to extend superposition model analysis to the fourth-rank ZFS terms for Fe^{3+} centers in h-$BaTiO_3$.

(Some figures in this article are in colour only in the electronic version)

1. Introduction

Barium titanate $BaTiO_3$ is one of the most used ferroelectric materials due to a wide range of technological applications. There exist two forms of barium titanate: normal (cubic) c-$BaTiO_3$ and hexagonal polymorph h-$BaTiO_3$, having different crystallographic structure. Over the years huge amounts of data have been collected on c-$BaTiO_3$, both pure as well as doped with various transition ions, as reviewed e.g. in the recent book [1]. However, data concerning h-$BaTiO_3$ are less numerous in literature. Electron magnetic resonance (EMR) [2–4] is a powerful spectroscopic technique to study the local distortions and defects in crystals using various paramagnetic $3d^N$ ions, e.g. Fe^{3+}, as spin probes. EMR

[1] Author to whom any correspondence should be addressed.

studies provide, among others, information about positions and local site symmetry of dopant ions in host lattice. However, adopting the proper form of spin Hamiltonian, and subsequent interpretation of the zero-field splitting (ZFS) parameters (ZFSPs) and Zeeman electronic ones is of paramount importance [2, 3]. A recent comparative analysis [5] of EMR data on Fe^{3+} ions doped in c-$BaTiO_3$ [6–10], has revealed that the truncated form of the fourth-rank ZFS terms used in [6] has led to controversy and misinterpretations of ZFSPs. The study [5] has also provided motivation for the present investigations.

In this paper we consider EMR data [11, 12] for the Fe^{3+} ions in h-$BaTiO_3$, which exhibits different spectroscopic properties and temperature behavior as compared with c-$BaTiO_3$. A crystal of c-$BaTiO_3$ undergoes three successive phase transitions [6–10]. At around 408 K it undergoes a paraelectric to ferroelectric transition from the cubic $Pm3m$ to the tetragonal $P4mm$ structure; at 278 K it becomes orthorhombic, $C2mm$; and at 183 K, a transition into the rhombohedral low-temperature phase $Rm3$ occurs [13]. Recently, order–disorder phenomena have been studied [13] in the low-temperature phase of c-$BaTiO_3$. The temperature behavior of the crystallographic structure of h-$BaTiO_3$ is quite different. X-ray investigation [14] of h-$BaTiO_3$ indicate that above $T_0 = 222$ K it is paraelectric described by hexagonal space group $P6_3/mmc$. At intermediate temperatures, i.e. $T_0 < T < T_C$, the structure is orthorhombic (space group $C222_1$), whereas below $T_C = 74$ K, a phase transition to the ferroelectric monoclinic phase (space group $P112_1$) occurs [15, 16].

EMR studies [11, 12] of the Fe^{3+} ions doped in h-$BaTiO_3$ indicate distinct and more complicated spectra than for the Fe^{3+} in c-$BaTiO_3$. Only one type of octahedral cluster TiO_6, which is corner-connected, exists in c-$BaTiO_3$; this constrains the possible positions of the doped $3d^N$ ions replacing Ti ions. As depicted in figure 1, the Ti ions in each hexagonal unit cell of h-$BaTiO_3$ occupy two crystallographically inequivalent sites: (1) in face-sharing Ti_2O_9 octahedra with four magnetically inequivalent sites and (2) in corner-sharing TiO_6 octahedra with two magnetically inequivalent sites [15–17]. Octahedra in h-$BaTiO_3$ are trigonally distorted along the c-direction [16] (see figure 1). The strength of the trigonal distortion differs for the two types of octahedral clusters. Studies [11, 12, 15] indicate that paramagnetic ions in h-$BaTiO_3$ more likely occupy the Ti sites in Ti_2O_9 than TiO_6 cluster. EMR studies [11, 12], of the Fe^{3+} doped in h-$BaTiO_3$ appear to indicate that the local environment of paramagnetic ions in Ti_2O_9 clusters is 'approximately' orthorhombic in all structural phases that occur with decreasing temperature.

Unfortunately, the EMR spectra arising from low symmetry centers are complex and can be misinterpreted by superficial analysis. Interpretation of EMR spectra [11, 12] was especially cumbersome due to existence of twins in the crystal and several magnetically inequivalent sites. The authors [11, 12] have carried out a meticulous and tedious analysis of EMR spectra based on an orthorhombic symmetry approximation, which is appropriate for temperatures above

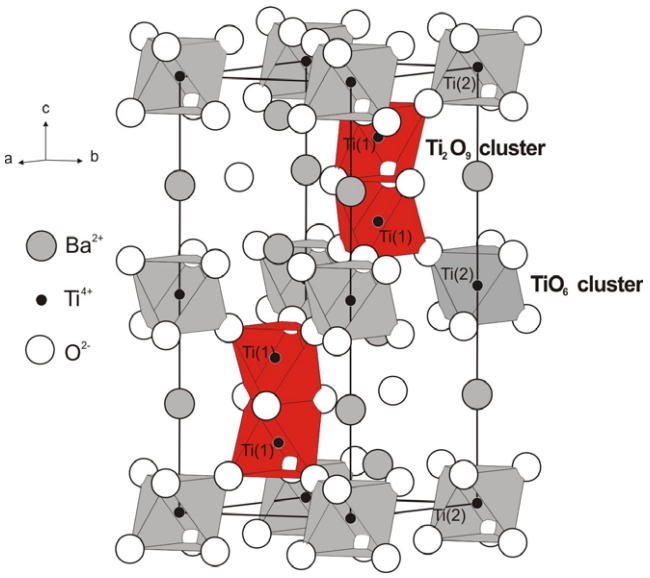

Figure 1. Unit cell of h-$BaTiO_3$ with the two types of Ti clusters indicated (adapted from [15]). The four magnetically inequivalent $Ti(1)_i$ sites, $i = 1, 2, 3$, and 4, are described by fractional positions at room temperature [14] $(x/a, y/b, z/c)$: (1/3, 2/3, 0.846 33), (1/3, 2/3, 0.653 67), (2/3, 1/3, 0.346 33), and (2/3, 1/3, 0.153 67), respectively.

$T_C = 74$ K. A major aim of this study is to consider an alternative interpretation of EMR data [11, 12] which enables investigation of the low symmetry aspects arising with the lowering of temperature during the orthorhombic to monoclinic structural phase transition in h-$BaTiO_3$ doped with Fe^{3+} ions. The results [11, 12] serve as a starting point for the present study. Interestingly, a Science Citation Index search reveals the papers [11, 12] have been cited in only a few cases and no follow-up EMR studies have appeared. Importantly, recent EMR studies of Cr^{3+} [15] and Mn^{4+} [16] ions doped in h-$BaTiO_3$ indicate specific peculiarities, which shed new light on the results [11, 12] and call for their reconsideration. The Cr^{3+} ion was observed at both Ti(1) and Ti(2) sites, whereas the overall XRD-measured phase composition of the ceramic samples investigated amounted to 11% tetragonal and 89% hexagonal phase [15]. A random distribution of ZFSPs ΔD and ΔE approximated by symmetric Gaussian function was assumed [16] to explain the EMR spectra of Mn^{4+}:h-$BaTiO_3$. The manganese ions may occur in various valence states: 4+, 3+, and 2+ and each ion type of ions may preferentially enter specific sites in h-$BaTiO_3$ [15]. Hence, the question: at which Ti lattice sites and in which valence states are the paramagnetic ions incorporated into h-$BaTiO_3$?, remains an open problem. Further EMR experimental and theoretical modeling studies of h-$BaTiO_3$ doped with various $3d^N$ ions may help in solving this question.

Earlier studies of pure and doped hexagonal $BaTiO_3$ investigated also optical [18], ESR [19–21], dielectric [22, 23], pressure [24, 25], x-ray [26], Mössbauer [27], and neutron diffraction [28] properties around the structural phase transitions. The studies [18–28] of the h-$BaTiO_3$ based materials have been driven by possibility of extending

the range of commercial applications of $BaTiO_3$. For example, the h-$BaTiO_3$ based ceramics due to their characteristics (dielectric constant, quality factors, coefficient of resonant frequency, temperature coefficient, ferroelectric properties, piezoelectricity) are widely used in capacitors, as chemical sensors, in piezoelectric devices, and as microwave materials [29]. One of the newest applications of h-$BaTiO_3$ is as a base of nanoferroelectric materials characterized by colossal dielectric constant (values up to 10^5) [30]. To study the particle size effects on the spin Hamiltonian parameters in nanopowders, the spectroscopic properties of single crystals must be well understood. This need, and the peculiarities [15, 16] of EMR for other transition ions doped in h-$BaTiO_3$, have prompted us to reexamine the EMR data [11, 12] for Fe^{3+}:h-$BaTiO_3$.

The organization of the paper is as follows. In section 2 we consider the spin Hamiltonian forms and notations used in the analysis of EMR spectra of Fe^{3+}: h-$BaTiO_3$ [11, 12]. Some discrepancies or misinterpretations identified by us, as well as their implications for interpretation of ZFS parameters, are clarified. In section 3 the definitions of pertinent axis systems and procedure for determination of the ZFSPs from EMR spectra are critically assessed. This enables reanalysis of the second- and fourth-rank ZFSPs determined by EMR and the second-rank ZFSPs computed using the superposition model for the Fe^{3+} ions in h-$BaTiO_3$ [11, 12]. The available ZFSPs expressed in different notations are presented in a well-defined axis system and in a unified way to ensure meaningful comparison. Pertinent transformations of ZFSPs are carried out using the package CST [31, 32], which facilitates conversions, standardization, and transformations of ZFS parameters (as well as crystal-field ones). Simulations of the low symmetry ZFS parameters are carried out to assess the role of the monoclinic and triclinic ZFS terms for interpretation of EMR data concerning the orthorhombic to monoclinic structural phase transition in Fe^{3+}:h-$BaTiO_3$. A summary and conclusions are provided in section 4.

2. Spin Hamiltonian forms pertinent to Fe^{3+} ($S = 5/2$) ions in hexagonal $BaTiO_3$

For transition-metal ions at triclinic symmetry (C_1 and C_i) sites in crystals the ZFS part in spin Hamiltonian [2–4] can be expressed in the compact form [33] in the extended ($-k \leqslant q \leqslant +k$) Stevens operator notation [34, 35] as:

$$\tilde{H}_{\rm ZFS} = \sum_{kq} f_k b_k^q O_k^q(S_x, S_y, S_z), \qquad B_2^q = \tfrac{1}{3} b_2^q \quad \text{and} \quad B_4^q = \tfrac{1}{60} b_4^q, \tag{1}$$

where f_k are the scaling factors, b_k^q and B_k^q—the ZFSPs, O_k^q—the extended Stevens operators [34, 35]. Note that the conventional Stevens operators [2–4] originally defined in [36] are limited to positive $q (0 \leqslant q \leqslant k)$ and cannot describe the low symmetry aspects [33]. Explicit listings of the extended Stevens operators are available in the literature for the most useful even ranks $k = 2$, 4, and 6, see, e.g. [37] (for other pertinent references, see [34, 35]), whereas an explicit listing for $k = 3$, 5, and 7 (both positive and negative values of q) is provided in [35], where these operators have been generalized to any rank k. The problems that arise from inconsistent or missing factors f_k occurring in some papers were discussed in [38]. For analysis of the results below we also provide the rotational invariants S_k defined [34] as $(S_k)^2 = \frac{1}{2k+1} N_k$ via the norms $N_k = \{b_k^0\}^2 + \sum_{q=1}^{k} (\frac{1}{c_q^k})^2 (\{b_k^q\}^2 + \{b_k^{-q}\}^2)$ of the ZFS parameters in equation (1), where the coefficients c_q^k are listed in [33, 34]. The quantities S_k are invariant with respect to an arbitrary rotation of the axis system and measure the ZFS 'strength'.

For monoclinic symmetry (C_2, C_s, C_{2h}) sites, where only one symmetry axis C_2 (or direction) exists, the most common choice $C_2 \parallel z$ yields [39, 40]:

$$\tilde{H}_{\rm ZFS} = B_2^0 O_2^0 + B_2^2 O_2^2 + B_2^{-2} O_2^{-2} + B_4^0 O_4^0 + B_4^2 O_4^2 + B_4^{-2} O_4^{-2} + B_4^4 O_4^4 + B_4^{-4} O_4^{-4}. \tag{2}$$

The two alternative choices, i.e. $C_2 \parallel y$ and $C_2 \parallel x$, correspond to different forms of ZFS Hamiltonian in equation (2) with the monoclinic terms for a given $k (|q| \leqslant k) : q = 1$, 3 and $q = -1, -3$, respectively [39, 40]. The orthorhombic form is obtained by neglecting in equation (2) the monoclinic ZFSPs with $q < 0$.

Contrary to the prevailing conventions [33, 41, 42] Shimokoshi and Ohi [12] represent the ZFS Hamiltonian (their equation (1)) as

$$H = g\beta H S + H_c, \qquad H_c = b_2^{0'} O_2^{0'} + b_2^{2'} O_2^{2'} + \tfrac{1}{60}(b_4^0 O_4^0 + b_4^2 O_4^2 + b_4^4 O_4^4). \tag{3}$$

In equation (3) we have added a prime to the superscript to distinguish the original operators and ZFSPs of [12] from the well-defined ZFSPs in the conventional or extended Stevens notation [2–4, 33–42]. Note that the terminology naming the actual ZFSPs bkq as the 'crystal-field' parameters in [12] or the ZFSP D as 'axial crystalline field' in [15] and [16] is inappropriate, since the crystal-field quantities and the ZFS ones have a distinct physical origin, and thus a meaning, as discussed in the reviews [33, 41].

An ambiguity arises concerning the scaling factors $f_2 = \frac{1}{3}$ [38], apparently missing in equation (3). Either they have been inadvertently omitted or definitions in [12] of either the operators $O_2^{m'}$ or ZFSPs $b_2^{q'}$ might differ from the standard ones [33–38]. The ZFSPs $b_2^{q'}$ in equation (3) resemble the orthorhombic B_2^q commonly defined [2–4, 33–42] as:

$$H_{\rm orth} = B_2^0 O_2^0 + B_2^2 O_2^2 + B_4^0 O_4^0 + B_4^2 O_4^2 + B_4^4 O_4^4. \tag{4}$$

Hence the values of b_2^0 and b_2^0 in [12] may be easily misinterpreted. The ZFS Hamiltonian form appropriate for triclinic symmetry is also used in [12] (their equation (2)), which disregards the scaling factors [38] in equation (1):

$$H_c' = \sum_{m=-2}^{2} b_2^{m'} O_2^{m'}. \tag{5}$$

The operators $O_2^m(S_x, S_y, S_z)$ were explicitly defined in [12] for $m = 0, \pm 1, \pm 2$, so without any reference to the

existing well-established definitions of the extended Stevens operators—see [33–42] and references therein. As exemplified in [33, 38, 42], usage in the EMR literature of the same symbol with different meanings has led to misinterpretations of the experimental ZFSP values. Introducing yet another operator notation, as in [12], is superfluous and adds to the existing confusion regarding spin Hamiltonian notations [33, 38, 42]. Checking the original definitions of O_2^m in equation (3) of [12] reveals that the scaling factors were incorporated into the operators. As a consequence, O_2^m in [12], i.e. $O_2^{m'}$ in equations (3) and (5), differ from the conventional Stevens operators [33–35], whereas $b_2^{m'}$ conform to the usual definitions [2, 3, 33–42] of b_2^q in equation (1), i.e. the following relations hold: $O_2^{m'} = f_2 O_2^q$, $f_2 = \frac{1}{3}$, and $b_2^{m'} = b_2^q$.

The authors [12] have also provided the relationships (their equations (8)) between the components D_{ij} of the D tensor ($\mathbf{S} \cdot \mathbf{D} \cdot \mathbf{S}$) and $b_2^{m'}$ in equation (5) as well as between the conventional ZFSPs D and E and the diagonalized components D_i' ($i = x, y, z$) expressed in the principal axis system of the 2nd-rank ZFS terms (their equations (11)): $D = \frac{3}{2}D_z'$, $E = \frac{1}{2}(D_x' - D_y')$. Comparison of equations (8) in [12] and those available in literature [38] indicate the correctness of the D_{ij} relationships [12].

A doubtful point concerns the conventional spin Hamiltonian form used in [11] (their equation (1)):

$$H = g\beta H S + D\left[S_z^2 - \tfrac{1}{3}S(S+1)\right] + E(S_x^2 - S_y^2) + \frac{a}{6}\left(S_x^4 + S_y^4 + S_z^4 - \frac{1}{5}S(S+1)(3S^2+3S-1)\right). \quad (6)$$

Equation (6) represents a truncated ZFS Hamiltonian, which has neither fully orthorhombic symmetry, then two 4th-rank ZFS terms [33] K (orthorhombic) and F (axial) must be included, nor tetragonal symmetry, then the E and K terms must be omitted and the F term must be added. The implications of the inconsistent spin Hamiltonian notations in [11] and [12] discussed above are considered in section 3.

3. Reanalysis of ZFS parameters for Fe^{3+} ions in h-$BaTiO_3$

3.1. Analysis of original experimental data

X-band EMR measurements [11] were carried out in the temperature range 283–163 K and truncated ZFSP sets were determined at 283 and 173 K. The measurements [11] were extended [12] down to 5 K and five orthorhombic ZFSPs were determined additionally at 77, 63, and 5 K. In both studies [11, 12] the isotropic $g = 2.00$ was assumed in fittings. EMR spectra seems to indicate two and three magnetically inequivalent axial and orthorhombic Fe^{3+} centers in h-$BaTiO_3$ in the room temperature and intermediate phase, respectively, which were ascribed to Fe^{3+} ions replacing Ti^{3+} in Ti_2O_9 clusters [11, 12]. In view of the inconsistent spin Hamiltonian notations discussed in section 2, the original ZFSP sets [11, 12] are converted as appropriate and presented in table 1 in a unified way in the two notations. The ZFSPs F, a, and K are calculated using the inverse conversion relations [5, 33]: $b_4^4 = \frac{5a}{2}$, $b_4^0 = \frac{a}{2} + \frac{F}{3}$, $b_4^2 = 60$ K, whereas the conventional

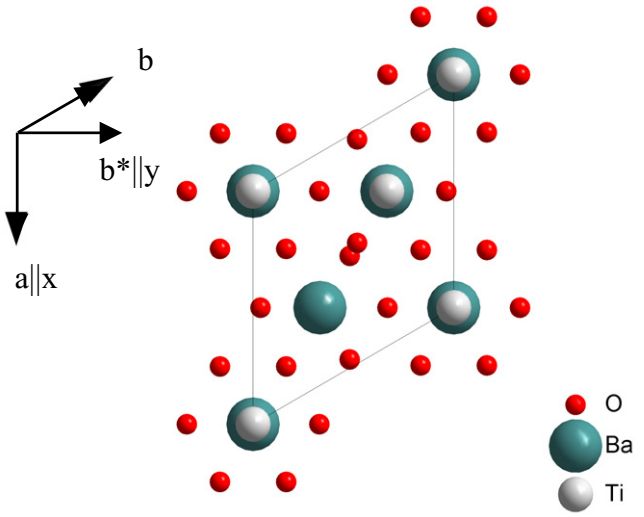

Figure 2. Projection of the unit cell onto the *ab*-plane indicating the laboratory axis system (x, y, z) w.r.t. the modified crystallographic axis system (a, b^*, c) as inferred by us from descriptions in [11, 12]; the z-axis, parallel to the c-axis, points out-of-plane.

ZFSPs [11, 12] are converted to the extended Stevens notation using the relations [5, 33]: $b_2^0 = D$, $b_2^2 = 3E$. The values of the rotational invariants S_k (see table 1) increase with temperature decreasing from room temperature to T_C, whereas they decrease below T_C. The procedure of extracting ZFSPs from EMR spectra as well as the theoretical modeling [11, 12] involves aspects related to specific symmetry constraints and transformation properties of H_{ZFS}. Since these aspects bear on interpretation of data and their reliability, they require clarifications as discussed below.

Crucial for these considerations is the question in which axis systems the ZFSP sets are expressed. In figure 2 we visualize the laboratory axis systems used in [11, 12]. Since the hexagonal crystallographic axis system at room temperature, i.e. (a, b, c), does not form a Cartesian axis system, a modified crystallographic axis system (a, b^*, c) has been adopted to conform with the axis systems used in [11, 12]. Then, the orientation of the laboratory axis system, i.e. (x, y, z), w.r.t. the modified crystallographic axis system could be inferred from descriptions in [11, 12] as follows: $z \parallel c$, $y \parallel b^*$, and $x \parallel a$. We have adopted the laboratory axis system used in both in [11, 12] as corresponding to a right-hand side axis system, so in figure 1 of [11] the z-axis appears to correspond to a left-hand side axis system, whereas the direction cosines in [11] are defined in a right-hand side axis system. In the unit cell of h-$BaTiO_3$ at room temperature there are two crystallographically inequivalent sites both trigonally distorted: Ti(1) and Ti(2), with four and two magnetically inequivalent sites, respectively [14, 15]. Hence, in fact, the trigonal form of H_{ZFS} should be used, instead of the orthorhombic form. The corresponding symmetry-adapted axis system, as defined in [40], may only approximately be determined from crystallographic data at room temperature, whereas no such data are available at lower temperatures. Considering the defect nature of the Fe^{3+} centers in h-$BaTiO_3$, the experimentally determined principal axis system of the

Table 1. The original ZFS parameters (in units of cm^{-1}) for the Fe^{3+} in h-$BaTiO_3$, and recalculated ones using appropriate relations (see text). Dash (—) means values were not determined. For set 6 and 7: b_4^0 and b_4^4 are recalculated assuming $F = 0$, whereas Euler angles (α, β, γ) are recalculated using the direction cosines given in [11].

Set	D	E	a	F	K	b_2^0	b_2^2	S_2	b_4^0	b_4^2	b_4^4	S_4	T (K)	α, β, γ (deg.)	Ref.
1	−0.058	0.0003	0.00212	0.01032	0.00003	−0.05800	0.00090	0.02594	0.0045	0.0015	0.0053	0.00153	283	90, 3, −90	[12]
2	−0.061	0.0046	−0.00480	0.02130	−0.00014	−0.06100	0.01380	0.02751	0.0047	−0.0085	−0.012	0.00182	173	−92, 5, 0	[12]
3	−0.063	0.012	−0.00480	0.01980	0.00033	−0.06300	0.03600	0.02967	0.0042	0.020	−0.012	0.00215	77	−90, 10, 0	[12]
4	−0.063	0.012	0.00048	0.01488	−0.00005	−0.06300	0.03600	0.02967	0.0052	−0.0027	0.0012	0.00175	63	−129, 11, 63	[12]
5	−0.062	0.0089	0.00164	0.00984	0.00020	−0.06200	0.02670	0.02857	0.0041	0.012	0.0041	0.00165	5	−150, 6, 90	[12]
6	−0.059	0.0001	0.0059	—	—	−0.05900	0.00030	0.02639	0.00295	—	0.01475	0.00129	283	90, −8, 0	[11]
7	−0.059	0.0046	0.0051	—	—	−0.05900	0.01380	0.02663	0.00255	—	0.01275	0.00111	173	90, −12, 0	[11]

2nd-rank ZFS terms may, to a large extent, correspond to the symmetry-adapted axis system.

Analysis of data in the figures and tables in [11, 12] reveals the following. The direction cosines provided for the principal axis system in table I of [11] yield axes that do not coincide with the axes depicted in figure 5 of [11]. Data for temperature 283 and 173 K in table I of [11] indicate the direction cosines yielding Euler angles, in degrees, (90, −8, 0) and (90, −12, 0), respectively. However, the Euler angles read out from the schematic axes in figure 5a of [11], corresponding to the axis systems denoted by ($X2$, Y, $Z2$) and ($X1$, Y, $Z1$), are (90, $+\beta$, 0) and (90, $-\beta$, 0), respectively, while the direction cosines for the principal axis system provided in table I of [11] correspond only to the axis systems denoted by ($X1$, Y, $Z1$). Similarly, Euler angles for the principal axis system in table 1 in [12] do not coincide with Euler angles read out from the schematic axes depicted in figure 3 of [12]. The latter Euler angles are (0, 0, 0) in the temperature range $T_0 = 222$ K to $T_C = 67$ K, whereas for the two sites observed below $T_C = 67$ K they are ($+\alpha$, 0, 0) and ($-\alpha$, 0, 0), with the value of α increasing to maximum $\alpha = 30°$ at $T = 51$ K, corresponding to the axis systems denoted by (X'', Y'', Z) and (X', Y', Z), respectively. Note that the Euler angles (α, β, γ) discussed above have been experimentally determined in [11, 12] w.r.t. the laboratory axis system by fitting EMR spectra.

Analysis of the original EMR spectra in [11] at room temperature and intermediate phases raises some doubts concerning the spectra interpretation by the authors [11, 12]. Crystallographic data at room temperature indicate that the local symmetry at the Ti(1) site is trigonal C_{3v}, with a three-fold axis parallel to the crystallographic c-axis. The observed angular dependences of the resonance field at room temperature phase, see figure 2 in [11], change with the direction of magnetic field in the xz- and yz-plane, while the lines are constant in the xy-plane. In the yz-plane two equivalent sets of lines are observed with mirror symmetry at the y- and z-axis, and the peak of each set shifts 8° from the y- and z-axis. On the other hand, only one set of lines is observed in the xz-plane. One line in the xz- and xy-plane corresponds to the axis y and z, respectively, which is parallel to a specific symmetry operation of trigonal point symmetry group C_{3v}, namely, mirror plane parallel to the rotation axis and the three-fold rotation axis, respectively. However, there are two equivalent sets of lines in the yz-plane. This is due to the fact that the x-axis is not parallel to the symmetry operation of C_{3v}. These results indicate that Fe^{3+} centers located at trigonal Ti sites at room temperature phase preserve the host trigonal symmetry. In the intermediate phase one line splits into three lines in the xz- and xy-plane. The three lines in the xy-plane are shifted by 60° w.r.t. each other. These results can be interpreted by the existence of Fe^{3+} centers located at monoclinic or lower symmetry sites.

The experimental principal values of ZFSPs D, E, and a provided in table I of [11] have been determined from EMR spectra, which were ascribed as follows. For temperature 283 K, two magnetically inequivalent, supposedly axial, sites were indicated with the Z-axis denoted by $Z1$ and $Z2$ in a direction −8° and +8° from the c-axis in the bc-plane, respectively. An increase of the angle between the Z-axis, i.e. the principal axis of the 2nd-rank ZFS terms, and the c-axis was observed with decreasing temperature in the intermediate phase ($T_0 < T < T_C$) from 8° at T_0 to 12° at 173 K. However, ZFSPs determined at temperature 173 K are described as due to not two but three magnetically inequivalent orthorhombic sites. The origin of the third such site cannot be explained based on the available crystallographic data (see above) and may be due at best to additional defects arising during substitution, or at worst to a misinterpretation of EMR spectra.

Due to truncation of H_{ZFS} in [11], comparison of the 4th-rank ZFSPs in table 1 recalculated from [11] and [12] is somewhat ambiguous. Moreover, all ZFSP sets in table 1 are, strictly speaking, not directly comparable (see below). Nevertheless, table 1 reveals the role of truncation of ZFSPs to (D, E; a) in [11] as compared with the full orthorhombic sets (D, E; b_4^0, b_4^2, b_4^4) in [12]. This role is evident in the disparities between the corresponding principal ZFSP values as well as the respective Euler angles determined in both papers at the same temperature T, i.e. 283 and 173 K. The respective Euler angles in table I of [12] disagree with the Euler angles recalculated by us from the direction cosines given in [11]—see values listed in table 1. We observe that D and a is roughly constant between the two temperatures, whereas a large change is revealed in E. Such a temperature dependence of ZFSPs also indicates a pronounced role of distortions of symmetry lower than axial, so no definite conclusions can be reached on that basis concerning the strength of possible monoclinic or triclinic distortions. Since the laboratory axis system used in both papers [11, 12] is the same, possible reasons for the disparities in the corresponding ZFSP values may be due to differences in the assignments of EMR spectra and fitting procedure used in [11] from those in [12].

Specific comments concerning ZFSP values of [11] and [12] are pertinent. The procedure for determination of ZFSP in [12] is based on the spin Hamiltonian in equation (3), where the coordinate system was chosen to make the 2nd-rank ZFS terms (D, E) diagonal. This coordinate system has, in fact, the meaning of principal axis system with the axes determined experimentally and described by respective Euler angles w.r.t. the modified crystallographic axis system (a, b^*, c), to which the laboratory axis system is directly related as ($z \parallel c$, $y \parallel b^*$, $x \parallel a$). Hence, the 2nd-rank ZFSPs in table I of [11, 12] represent the principal values expressed in the respective experimentally determined principal axis systems for a given temperature. The least squares fittings [11], based on a truncated spin Hamiltonian in equation (6), yielded the fitted values of ZFSPs (D, E; a), whereas the respective direction cosines in their table 1 appear to be experimentally determined. Since the angle between the principal Z-axis of the 2nd-rank ZFS terms and the c-axis changes with temperature in the intermediate phase, the experimental values of (D, E; a) at 283 and 173 K in table I of [11] are expressed in different principal axis systems. Thus, such sets cannot be fully directly compared. Direct comparison of such principal values may only provide an overall assessment of the relative strength of the 'diagonalized' ZFSPs for various magnetically inequivalent yet crystallographically equivalent

sites. However, the orientation of the principal axes is not taken into account in such comparison. To ensure comprehensive direct comparability of such ZFSP sets and more importantly to consider the low symmetry aspects, it is useful to back transform the original ZFSP values from table I in [11] and [12] to a common axis system using the direction cosines provided. The back transformations of ZFSP sets are carried out in section 3.2.

A question arises whether all corresponding but independently measured ZFSP sets in [11, 12] refer to the same magnetically inequivalent site with a particular orientation in the unit cell. Only if it is the case will the back transformation of the original ZFSP values from a specific axis system to a common axis system using the direction cosines provided yield comparable sets. Otherwise one would obtain disparate, i.e. non-comparable sets. Judging by the temperature variation of Euler angles from 283 to 5 K, doubts arise if this condition is really met. In particular, there is no smooth variation of Euler angles between $T = 283$ and 173 K, as well as between $T = 77$ and 63 K. However, we are not in a position to solve this question without access to raw experimental data.

The assumption in [12] that the *'principal axes of 4th-rank term coincide with that of the second order'* is physically incorrect since the principal axes can only be defined for the 2nd-rank ZFS terms. Least squares fittings enabled determination [12] of the ZFSPs listed in their [12] table 1 and their temperature dependence. Some ambiguities were encountered in determination of the 4th-rank ZFSPs and no rules concerning their temperature dependence could be found [12]. In fact, only b_4^0 shows a regular behavior, whereas b_4^2 and b_4^4 reveal rather erratic variation with temperature (see table 1). Below 51 K no temperature dependence of EMR spectra was observed.

A crucial aspect concerns the monoclinic ZFSPs, discussed in section 2, which were not included in the procedure used in [11] and [12]. In fact, for monoclinic symmetry, diagonalization of the 2nd-rank ZFS terms, should leave all orthorhombic as well as monoclinic 4th-rank ZFSPs non-zero. Therefore, the usage of only the orthorhombic sets (b_4^0, b_4^2, b_4^4) in [12] for temperatures below $T_C = 74$ K must be considered as an approximation. The omission of the 4th-rank monoclinic ZFSPs may affect the fitted values of the orthorhombic ZFSPs, which reveal rather erratic variation with temperature as discussed above. These aspects are discussed in detail in section 3.2.

3.2. Low symmetry aspects

To ensure comprehensive direct comparability of the original ZFSP sets [11, 12] in table 1, the back transformations discussed in section 3.1 must be carried out. For this purpose, the direction cosines [11] and the Euler angles [12] are used within the package CST [31, 32] to transform the original ZFSPs of table 1 to the laboratory axis system (x, y, z) by the appropriate inverse transformations $(-\gamma, -\beta, -\alpha)$. The so-obtained back transformed ZFSP sets are listed in table 2. The results enable analysis of the influence of lower symmetry distortions of the local environment around the paramagnetic ion and hence consideration of the low symmetry aspects involved. This procedure also enables direct comparison of the ZFSPs experimentally determined at various temperatures [11, 12] and facilitates comparison with the ZFSPs for Fe^{3+} in c-$BaTiO_3$.

It should be kept in mind that the 'diagonalized' ZFSPs in table 1 are expressed in the experimentally determined principal axis system of the 2nd-rank ZFSPs. Hence, due to the orthorhombic approximation used they may not represent the actual low symmetry ZFSPs, which may occur especially for the sets 4 and 5. Hence, the triclinic-like ZFSPs appearing after the reverse rotation $(-\gamma, -\beta, -\alpha)$ may not reflect the actual strength of low symmetry distortions. A more reliable procedure could involve fitting EMR spectra measured in a well-defined axis system, e.g. (a, b^*, c), with all triclinic ZFSPs included. Then diagonalization of the 2nd-rank ZFSPs could be performed to find their principal values and the corresponding principal axis system defined by Euler angles w.r.t. (a, b^*, c). In general, the pseudosymmetry axes method [43] could be applied to consider the appropriate higher symmetry approximation for the 4th-rank ZFSPs and the relationships of the pseudosymmetry axes with the metal–ion ligand bonds [44]. These results could be then compared with those determined from EMR spectra by a different route in [11] and [12]. However, in the present case the orthorhombic approximation within the pseudosymmetry axes method [44] must yield the same results as those obtained in the principal axis system of the 2nd-rank ZFSPs. This expectation has been verified by direct calculations.

If we compare sets 1 and 6 or 2 and 7 from table 2, obtained under the same conditions (i.e. axis systems and temperature), serious inconsistencies may be noticed between the values of ZFSPs, which in principle should be quite comparable. Values of b_4^0 determined in [12] and these from [11] for 283 and 173 K (sets 1, 2 and 6, 7 in table 2) after rotation to the same (initial) axis system differ by about 50%. A closer look at the values of b_2^0 in table 1 for a given temperature reveal an apparent consistency, with difference of about 0.001 cm^{-1}, but one must remember that these data are expressed in different axis systems, i.e. they are described by different Euler angles. Since the same definitions of the modified crystallographic axis system and equivalently the laboratory axis system have been consistently used in both papers [11, 12], the differences in Euler angles for supposedly comparable data sets revealed by our analysis may be due to either a different orientation of the magnetically inequivalent sites or the truncated form of H_{ZFS} used in [11]. After transformation to the same axis system (see, table 2) the values of b_2^0 for 283 K (sets 1 and 6) are very similar (difference of 0.0005 cm^{-1}), but for 173 K (sets 2 and 7) they differ by about 0.0054 cm^{-1}, i.e. 9%. More pronounced inconsistencies are noticed for the values of b_2^2, differing between set 2 and 7 by about 25%. Most probably the reason for such inconsistencies might be due to the usage of the truncated spin Hamiltonian form in [11].

Using the laboratory axis system (x, y, z) defined (see figure 2) w.r.t. to the modified hexagonal crystallographic axis system (a, b^*, c) at room temperature as $(z \parallel c, y \parallel b^*, x \parallel a)$,

Table 2. The ZFS parameters of table 1 (in units of cm^{-1}) after back transformation to the modified crystallographic axis system (a, b^*, c) using the inverse rotation $(\alpha', \beta', \gamma') = (-\gamma, -\beta, -\alpha)$.

Set	b_2^0	b_2^1	b_2^{-1}	b_2^2	b_2^{-2}	b_4^0	b_4^1	b_4^{-1}	b_4^2	b_4^{-2}	b_4^3	b_4^{-3}	b_4^4	b_4^{-4}	T (K)	$(\alpha', \beta', \gamma')$ (deg.)
1	−0.0578	—	−0.0181	0.0011	—	0.0044	—	0.0049	0.0013	—	—	0.0016	0.0053	—	283	90, −3, −90
2	−0.0603	0.0012	0.0342	−0.0130	0.0009	0.0045	−0.0004	−0.0102	0.0078	−0.0005	−0.0001	−0.0009	−0.0119	0.0017	173	0, −5, 92
3	−0.0596	—	0.0770	−0.0326	—	0.0040	—	−0.0041	−0.0191	—	—	0.0321	−0.0106	—	77	0, −10, 90
4	−0.0600	0.0309	0.0559	−0.0229	−0.0296	0.0043	−0.0100	−0.0143	0.0010	0.0044	0.0023	−0.0033	−0.0003	0.0012	63	−63, −11, 129
5	−0.0611	0.0287	0.0166	−0.0138	−0.0239	0.0038	−0.0104	−0.0060	−0.0054	−0.0093	0.0000	0.0102	−0.0019	0.0033	5	−90, −6, 150
6	−0.0573	—	0.0489	0.0014	—	0.0027	—	−0.0078	−0.0011	—	—	−0.0078	0.0145	—	283	0, 8, −90
7	−0.0549	—	0.0776	−0.0097	—	0.0020	—	−0.005	−0.0021	—	—	−0.0095	0.0122	—	173	0, 12, −90

Table 3. The set 2 ($T = 173$ K) ZFS parameters for Fe^{3+} at the site $Ti(1)_1$ of table 1 (2-PAS_1) and table 2 (2-LAS_1) transformed to other magnetically inequivalent sites using the respective Euler angles (α, β, γ) in degrees; PAS stands for 'principal axis system', LAS—for 'laboratory axis system'; Euler angles provided in the third column represent the reverse transformations of sets 2-LAS_i to the set 2-PAS_1.

$Ti(1)_i$	$(\alpha, \beta, \gamma)_i$	$(\alpha, \beta, \gamma)_{PAS1}$	b_2^0	b_2^1	b_2^{-1}	b_2^2	b_2^{-2}	b_4^0	b_4^1	b_4^{-1}	b_4^2	b_4^{-2}	b_4^3	b_4^{-3}	b_4^4	b_4^{-4}
2-PAS_1	—	0, 0, 0	−0.0610	—	—	0.0138	—	0.0047	—	—	−0.0085	—	—	—	−0.012	—
2-LAS_1	0, 0, 0	−92, 5, 0	−0.0603	0.0012	0.0342	−0.0130	0.0009	0.0045	−0.0004	−0.0102	0.0078	−0.0005	−0.0001	−0.0009	−0.0119	0.0017
2-LAS_2	0, 180, 0	92, −175, 0	−0.0603	0.0012	−0.0342	−0.0130	−0.0009	0.0045	−0.0004	0.0102	0.0078	0.0005	−0.0001	0.0009	−0.0119	−0.0017
2-LAS_3	180, 0, 0	88, 5, 0	−0.0603	−0.0012	−0.0342	−0.0130	0.0009	0.0045	0.0004	0.0102	0.0078	−0.0005	0.0001	0.0009	−0.0119	0.0017
2-LAS_4	180, 180, 0	−88, 185, 0	−0.0603	−0.0012	0.0342	−0.0130	−0.0009	0.0045	0.0004	−0.0102	0.0078	0.0005	0.0001	−0.0009	−0.0119	−0.0017

Euler angles describing transformations between the four magnetically inequivalent $Ti(1)_i$ sites are determined as: $Ti(1)_1$ to $Ti(1)_2 - (0, \pi, 0)$, $Ti(1)_1$ to $Ti(1)_3 - (\pi, 0, 0)$, and $Ti(1)_1$ to $Ti(1)_3 - (\pi, \pi, 0)$. It may be expected that these relations hold also at lower temperatures, however, the local environment undergoes some changes. For illustration, for set 2 (173 K) in tables 1 and 2 we consider the interrelationships between ZFSPs for the four magnetically inequivalent $Ti(1)_i$ sites. Taking the original ZFSPs in table 1 as corresponding to Fe^{3+} at the $Ti(1)_1$ site, first we back transformed these ZFSPs from the respective principal axis system to the laboratory axis system (table 2) and then we calculated the corresponding ZFSPs in the laboratory axis system for other three $Ti(1)_i$ ($i = 2$–4) sites. The results provided in table 3 indicate the respective sign changes for specific ZFSPs, whereas the magnitudes remain the same. Hence, the experimental observations of several magnetically inequivalent sites based on EMR spectra at a given temperature must be reconsidered, since they do not conform to the expected interrelationships evidenced in table 3.

Only three 4th-rank terms: b_4^0, b_4^2, and b_4^4, were employed, since it was assumed [12] that the local symmetry of Fe^{3+} ion was not much different from orthorhombic. For h-$BaTiO_3$ in the monoclinic phase below $T_C = 74$ K this approach may be considered only as an approximation since the actual symmetry experienced by Fe^{3+} ions is expected to be lower than orthorhombic. In fact, due to symmetry considerations as well as possible charge compensation mechanisms, the actual site symmetry at some Fe^{3+} defect centers in h-$BaTiO_3$ in the intermediate and monoclinic phase could be considered as triclinic. Group theory predicts distortions from trigonal local site symmetry not to the orthorhombic but directly to either the monoclinic or triclinic site symmetry [45]. In the triclinic case, all $-k \leqslant q \leqslant k$ ZFS components for $k = 2$ and 4 should be taken into account, whereas in the monoclinic case three 2nd-rank ZFSPs would be required. Thus keeping in mind the ascent in symmetry method [45], the experimentally determined orthorhombic 2nd-rank ZFSPs in their principal axis systems [12] may be considered only as an approximation.

In order to assess the influence of the low symmetry ZFS terms on the final experimental results, a simulation of the fitted ZFSP values has been carried out. Non-zero values of the ZFSPs representing lower than orthorhombic symmetry have been adopted as a certain percentage of the major orthorhombic ones—the results are given in table 4. The rationales for such simulation stems from the fact that the fittings should have been done using a full set of the 4th-rank ZFSPs when attempts to experimentally determine the principal axes of the 2nd-rank ZFS terms and the respective principal values.Having obtained the orthorhombic-like form of the 2nd-rank ZFS terms, either by diagonalization of the initial triclinic or monoclinic 2nd-rank ZFSP sets or experimental (so approximate) determination, in each case we would have obtained a full triclinic or monoclinic set of the 4th-rank ZFSPs expressed in the principal axes of the 2nd-rank ZFS terms, which themselves were referred to the modified crystallographic axis system. Hence, for the original sets 4 and 5 in table 1 we have supplemented the low symmetry 4th-rank ZFSPs by values equal to a moderate fraction of the respective b_4^0 value, for a trial we adopt a 25% factor. Three monoclinic cases (a: C2 $\parallel Z$, b: C2 $\parallel Y$, and c: C2 $\parallel X$) and triclinic case (d: TR) are considered in table 4. The supplemented sets are then back transformed to the modified crystallographic axis system (defined by: $\alpha = 0, \beta = 0, \gamma = 0$) using the respective inverse rotation $(-\gamma, -\beta, -\alpha)$. This procedure yields the respective sets marked in table 4 by $(*)$. The physical meaning of these sets pertains to the possible fitting outcomes, had originally full triclinic or monoclinic 4th-rank ZFSP sets been taken into account. Additionally, similar simulations have been carried out using various numerical factors to supplement the 'missing' low symmetry 4th-rank ZFSPs. However, in order to save space we refrain from providing the additional tables. A major conclusion from such simulations is clearly evident from table 4, even with the moderate 'filling factor' used. It turns out that the low symmetry 4th-rank ZFSPs when expressed in the modified crystallographic axis system takes on non-negligible values and thus significantly affect the fitting results. Therefore it would be advisable to carry out re-fittings of the original raw experimental data [12] using the full triclinic or at least monoclinic ZFSP set.

3.3. Analysis of superposition model calculations

Theoretical modeling based on the superposition model [37, 46] was carried out in [11, 12] only for the 2nd-rank ZFSPs. The modeling in [11] utilized specific assumptions. This includes equations from [10] pertaining to c-$BaTiO_3$, which also apply to h-$BaTiO_3$, the coordination number N and intrinsic parameter $\overline{b_2}(R_0)$ for MgO [47], and structural parameters [14] for h-$BaTiO_3$. Matching the theoretical ZFSPs with the experimental ones [11] yielded the calculated values in their table I. This modeling enabled evaluation of the shifts $(\Delta a, \Delta b^*, \Delta c)$ of Fe^{3+} ion w.r.t. the position of the host Ti(1) ion in the Ti_2O_9 cluster at temperatures 173 and 283 K. Using the crystallographic data [14] and $\overline{b_2}(R_0)$ [47], the ZFSPs D and E were plotted as a function of the shift Δc and Δb^* of the Fe^{3+} ion along the c- and b^*-axis, respectively [11]. The shift Δc corresponding to the experimental D value ($b_2^0 = D = -0.059$ cm^{-1}) was determined as either 0.017 or -0.033 nm for Fe^{3+} ion in the Ti_2O_9 cluster, whereas no matching could be obtained for Fe^{3+} ion in the TiO_6 cluster. The shift Δb^* corresponding to the experimental E value ($b_2^2 = 3E = 0.0046$ cm^{-1}) was determined as -0.0005 nm. The so-determined shifts Δc and Δb^* within the Fe: TiO_6 and Fe: Ti_2O_9 cluster have led to a conclusion that the superposition model rejects the hypothesis of a Fe^{3+} ion in a TiO_6 cluster, whereas it makes the smaller displacement Δc for the Ti_2O_9 cluster more plausible. However, this approach neglects the fact that any shift along the b^*-axis should result not only in a non-zero b_2^2, but all 2nd-rank ZFSPs should appear in this case. Hence, a triclinic form of H_{ZFS} should apply and not the orthorhombic one assumed in [11].

A closer analysis of the superposition model calculations [11, 12] reveals that the procedure used must be reconsidered for several reasons. Here we note only the critical points, of which the first two concern the superposition model calculations in [11, 12], whereas the points 3 to 5 and 6 concern only

Table 4. Simulation of the 4th-rank ZFS parameters for the sets 4 and 5 in table 1 (in units of cm^{-1}) by supplementing the low symmetry ZFSPs by values (*in italics*) equal to 25% of the respective b_4^0; the rationales for the monoclinic (a: C2 $\parallel Z$; b: C2 $\parallel Y$; c: C2 $\parallel X$) and triclinic (d: TR) symmetry cases are described in text; the supplemented sets are back transformed to the modified crystallographic axis system, for which Euler angles are ($\alpha = 0, \beta = 0, \gamma = 0$), using the inverse rotation ($-\gamma, -\beta, -\alpha$) yielding the respective sets marked by (*).

Case	Set	b_4^0	b_4^1	b_4^{-1}	b_4^2	b_4^{-2}	b_4^3	b_4^{-3}	b_4^4	b_4^{-4}
C2 $\parallel Z$	4a	0.0052	—	—	−0.0027	*0.0013*	—	—	0.0012	*0.0013*
	4a*	0.0043	−0.0100	−0.0150	0.0019	0.0037	0.0000	−0.0029	−0.0015	0.0012
C2 $\parallel Y$	4b	0.0052	*0.0013*	—	−0.0027	—	*0.0013*	—	0.0012	—
	4b*	0.0043	−0.0095	−0.0153	0.0006	0.0046	0.0014	−0.0028	−0.0002	0.0013
C2 $\parallel X$	4c	0.0052	—	*0.0013*	−0.0027	—	—	*0.0013*	0.0012	—
	4c*	0.0044	−0.0091	−0.0140	0.0008	0.0040	0.0018	−0.0042	−0.0004	0.0013
TR	4d	0.0052	*0.0013*	*0.0013*	−0.0027	*0.0013*	*0.0013*	*0.0013*	0.0012	*0.0013*
	4d*	0.0043	−0.0085	−0.0156	0.0013	0.0035	−0.0015	−0.0033	−0.0015	0.0013
C2 $\parallel Z$	5a	0.0041	—	—	0.012	*0.0010*	—	—	0.0041	*0.0010*
	5a*	0.0038	−0.0102	−0.0063	−0.0046	−0.0098	−0.0011	0.0102	−0.0028	0.0028
C2 $\parallel Y$	5b	0.0041	*0.0010*	—	0.012	—	*0.0010*	—	0.0041	—
	5b*	0.0038	−0.0099	−0.0068	−0.0056	−0.0092	−0.0009	0.0102	−0.0019	0.0033
C2 $\parallel X$	5c	0.0041	—	*0.0010*	0.012	—	—	*0.0010*	0.0041	—
	5c*	0.0038	−0.0096	−0.0055	−0.0055	−0.0095	0.0000	0.0093	−0.0019	0.0034
TR	5d	0.0041	*0.0010*	*0.0010*	0.012	*0.0010*	*0.0010*	*0.0010*	0.0041	*0.0010*
	5d*	0.0038	−0.0090	−0.0066	−0.0048	−0.0099	−0.0020	0.0093	−0.0027	0.0029

considerations in [11] and [12], respectively. *First*, probably the laboratory axis system (related to the modified crystallographic axis system) has been used in the superposition model calculations [11, 12], whereas the resulting D and E were directly compared with the experimental ZFSPs expressed in the principal axis system of the 2nd-rank ZFS terms. Thus, the theoretically and experimentally determined ZFSPs [11, 12], cannot be directly compared; the two ZFSP sets must be first transformed to a common axis system. This may generate additional low symmetry ZFSPs. *Second*, the relative orientation of the modified crystallographic axis system and the symmetry-adapted axis system should be identified. It appears that the axis system used in the superposition model calculations [11, 12], may differ from the actual symmetry-adapted axis system for the Fe^{3+} ions in h-$BaTiO_3$. If it really is the case, two options may be adopted. Either (1) using the crystallographic data [14] one could calculate a triclinic ZFSP set in the modified crystallographic axis system and then transform these ZFSPs to the symmetry-adapted axis system to obtain the symmetry allowed ZFSPs as the only non-zero parameters, whereas lower symmetry ZFSPs may be expected to reduce to zero, or (2) the crystallographic data, i.e. ionic positions, could be converted to the symmetry-adapted axis system and then one could calculate only a trigonal ZFSP set since the actual site symmetry of Ti^{3+} ions is trigonal: C_{3v} for Ti(1) sites in the Ti_2O_9 cluster, or D_{3d} for Ti(2) sites in the TiO_6 cluster. In the present case, any superposition model calculations based on the modified crystallographic axis system and not on the appropriate symmetry-adapted axis system would yield an incorrect set of ZFSPs as far as their magnitudes and symmetry are concerned.

Third, lowering of point group symmetry from trigonal to orthorhombic is not permitted by group theory [45], only a direct change to either monoclinic or triclinic site symmetry is permitted. Hence, appropriate forms of ZFS Hamiltonian should be used in the superposition model calculations in [11], which invoke the shifts Δc and Δb^*. *Fourth*, the structural model adopted in [11] assuming the shifts Δc, Δb^* and $\Delta a \equiv 0$ in the Ti_2O_9 cluster corresponds to a particular site symmetry, which has not been explicitly considered. This local site symmetry determines the appropriate form of ZFSPs to be used in superposition model calculations. *Fifth*, the non-zero shifts Δc, Δb^*, and possibly Δa change not only the local site symmetry of the Fe^{3+} centers in both clusters, but also necessitate moving the origin of the coordinate system to the central ion. Relaxation of the fixed positions of the Fe^{3+} ions replacing Ti^{3+} ions may be accompanied also by shifts of the surrounding oxygen atoms. Thus it would also be worthwhile considering appropriate alternative structural models.

Sixth, it appears that the ligand positions were not known in the intermediate and ferroelectric phase, hence only the room temperature crystallographic data have been employed in the superposition model calculations [12]. It is not clear if these data pertain to the TiO_6 cluster or the Ti_2O_9 cluster. Moreover, having more accurate data, better modeling could be performed. In the superposition model calculations [12], the relaxation of the oxygen positions as well as those of the Fe^{3+} ions was considered and the numerical values of the parameters u_{ij} and f_i describing these relaxations, respectively, were determined by the temperature dependence of the lattice constants. Although the D and E values determined by superposition model calculations compared well with the experimental ones, due to the approximations used to obtain them, this apparent agreement must be treated with caution.

In view of the critical points discussed above, we have embarked on a reconsideration of the superposition model calculations for the Fe^{3+} ions in h-$BaTiO_3$ [11, 12]. To clarify some aspects, initially we have partially repeated the superposition model calculations [11, 12]. Our results show, e.g., that the shifts $\Delta c = 0.017$ nm and $\Delta b^* = -0.0005$ nm yield similar values of b_2^0 and b_2^2 as obtained in [11, 12]. Moreover, as expected they indeed generate the non-zero triclinic symmetry 2nd- and 4th-rank ZFSPs not taken into

account in [11, 12]. Our preliminary superposition model calculations, although yielding different specific numerical results, seem to support the overall conclusion [11, 12] that the Fe^{3+} ions in Ti_2O_9 clusters yield better agreement with EMR data than that in TiO_6 clusters. Full details of more appropriate superposition model calculations taking into account all low symmetry aspects and extended to the 4th-rank ZFSPs will be given in a follow-up paper.

4. Summary and conclusions

This paper deals with the low symmetry aspects inherent in EMR studies of the orthorhombic to monoclinic structural phase transition in the hexagonal polymorph h-$BaTiO_3$ doped with Fe^{3+} ions. Previous experimental EMR results [11, 12], including the second- and fourth-rank zero-field splitting (ZFS) parameters determined by EMR and the second-rank ones computed using the superposition model for the Fe^{3+} ions in h-$BaTiO_3$ are thoroughly reanalyzed. Our reanalysis prompted clarification of the pertinent spin Hamiltonian notations and choices of the axis systems used in [11, 12]. To facilitate meaningful data comparison, available ZFS parameters are converted and presented in a well-defined axis system and in a unified way. The method of back transformations of the ZFS parameters experimentally measured in the principal axis system of the 2nd-rank ZFS terms to the laboratory axis system defined w.r.t. the modified crystallographic axis system appropriate for the hexagonal unit cell of h-$BaTiO_3$ has been employed. Pertinent transformations of ZFS parameters have been carried out using a versatile computer package CST for conversions, standardization, and transformations of ZFS parameters (as well as crystal-field ones). The role of the monoclinic and triclinic ZFS terms and the associated low symmetry aspects arising with lowering of temperature during the orthorhombic to monoclinic structural phase transition in Fe^{3+}:h-$BaTiO_3$ have been studied. For this purpose simulations of the low symmetry ZFS parameters were carried out assuming reasonable values of the ZFS parameters involved.

The procedure for analysis of experimental and theoretical ZFS parameters for transition ions at the monoclinic and triclinic symmetry sites proposed here has not been employed in earlier studies. Usefulness of this procedure is illustrated using, as a case study, the Fe^{3+} ions doped in h-$BaTiO_3$. Our considerations enable quantitative investigations and thus a better understanding of the low symmetry aspects in question. Importantly, such considerations may also help distinguishing the actual site symmetry from any approximations made in the process of extracting structural information from EMR spectra. It turns out that the monoclinic and triclinic ZFS terms arising from the lowering of temperature during the orthorhombic to monoclinic structural phase transition in h-$BaTiO_3$ doped with Fe^{3+} ions are quite pronounced. Hence, more detailed EMR studies of Fe^{3+}:h-$BaTiO_3$ are needed to verify the present predictions concerning the importance of the low symmetry aspects in question. This study suggests the need to extend the superposition model analysis for the Fe^{3+} centers in h-$BaTiO_3$ to the fourth-rank ZFS terms as well as to consider other possible Fe^{3+} centers in h-$BaTiO_3$. A more advanced superposition model of ZFS parameters for this ion-host system, including the fourth-rank ZFS terms, based on the procedure proposed here will be dealt with in a forthcoming paper. The proposed procedure for dealing with the low symmetry aspects involved in EMR spectra may find general applications in studies of various low symmetry ion-host systems.

Finally, it is worth mentioning also EMR studies of transition ions in c-$BaTiO_3$ and other crystals, which exhibit the hexagonal-$BaTiO_3$ type structure, e.g. $TlZnF_3$ and $RbZnF_3$. EMR studies of the Fe^{3+}–V_O (V_O—an oxygen vacancy) centers in c-$BaTiO_3$ ceramic samples doped with rare-earth ions [48] and various paramagnetic defects in $BaTiO_3$, including Fe^{4+}–V_O, and their role in light-induced charge transport [49] indicate importance of the g-factor for interpretation of experimental data and assignment of various centers. More accurate EMR studies of iron centers in h-$BaTiO_3$, taking into account the orthorhombic g-factors as well as the possible existence of Fe^{2+} and Fe^{4+} centers [50] could help to resolve better the low symmetry aspects discussed in this paper. Studies by Ebisu *et al* [51] of Cr^{3+} centers in $TlZnF_3$ reveal three kinds of Cr^{3+} spectra with trigonal symmetry. These centers were ascribed respectively to a charge-uncompensated Cr^{3+} ion at the Zn_2F_9 unit (Zn site II), a Cr^{3+} ion associated with a nearest Zn^{2+} vacancy at the Zn_2F_9 unit, and a charge-uncompensated Cr^{3+} ion at the ZnF_6 unit (Zn site I). EMR studies by Takeuchi *et al* [52] of vanadium centers in $RbZnF_3$ reveal one spectrum with cubic symmetry ascribed to a V^{2+} ion ($S = 3/2$) substituting for a host Zn^{2+} ion and another spectrum with tetragonal symmetry ascribed to a V^{4+}–O^{2-} pair ($S = 1/2$) substituting for the host Zn^{2+}–F^- pair in the cubic perovskite phase, whereas in the V, Li-codoped crystal two kinds of new EMR spectra with monoclinic symmetry with $S = 1/2$ and $I = 7/2$ were observed, and no V^{2+} centers were observed. EMR studies by Böttcher *et al* of Cr^{3+} [15] and Mn^{4+} [16] centers and most recent EMR, structural, and optical studies by Langhammer *et al* of Cr^{3+} [53] in h-$BaTiO_3$ indicate various EMR active centers at Ti(1) and Ti(2) sites. The recent EMR studies discussed above call for more comprehensive modeling of the zero-field splitting parameters for iron ions in the hexagonal form of $BaTiO_3$, i.e. considering iron ions at various other possible sites as well as in other valence states. Therefore, pertinent superposition model analysis, at first for Fe^{3+} ions, will be carried out in a subsequent paper.

Acknowledgments

This work was partially supported by the research grant from the Polish Ministry of Science and Higher Education in the years 2006-2009. Thanks are due to Drs A Mech and M Karbowiak for help in obtaining structural data used in this work.

References

[1] Rabe K M, Ahn C H and Triscone J-M (ed) 2007 *Physics of Ferroelectrics—A Modern Perspective* (Berlin: Springer)
[2] Abragam A and Bleaney B 1986 *Electron Paramagnetic Resonance of Transition Ions* (New York: Dover)

[3] Altshuler S and Kozyrev B M 1972 *Electron Paramagnetic Resonance in Compounds of Transition Elements* (Moscow: Nauka)
[4] Stevens K W H 1997 *Magnetic Ions in Crystals* (Princeton, NJ: Princeton University Press)
[5] Rudowicz C and Budzyński P 2006 *Phys. Rev.* B **74** 054415
[6] Decker D L, Huang K and Nelson H M 2002 *Phys. Rev.* B **66** 174103
[7] Sakudo T 1963 *J. Phys. Soc. Japan* **18** 1626
[8] Hornig A W, Rempel R C and Weaver H E 1959 *J. Phys. Chem. Solids* **10** 1
[9] Sakudo T and Unoki H 1964 *J. Phys. Soc. Japan* **19** 2109
[10] Siegel E and Müller K A 1979 *Phys. Rev.* B **20** 3587
[11] Ohi K, Arai H, Ishige T and Shimokoshi M 1989 *J. Phys. Soc. Japan* **58** 378
[12] Shimokoshi M and Ohi K 1990 *J. Phys. Soc. Japan* **59** 3629
[13] Völkel G and Müller K A 2007 *Phys. Rev.* B **76** 094105
[14] Evans H T Jr and Burbank R D 1948 *J. Chem. Phys.* **16** 634
[15] Böttcher R, Erden E, Langhammer H T, Müller T and Abricht H-P 2005 *J. Phys.: Condens. Matter* **17** 2763
[16] Böttcher R, Langhammer H T, Müller T and Abricht H-P 2005 *J. Phys.: Condens. Matter* **17** 4925
[17] Keith G M, Samar K, Alford N MCN and Sinclair D C 2004 *J. Electroceram.* **13** 305
[18] Akishige Y, Yokozeki N, Kobayashi M and Sawaguchi E 1986 *Solid State Commun.* **60** 445
[19] Ohi K, Arai H, Ishige T and Shimokoshi M 1989 *Ferroelectrics* **96** 3
[20] Langhammer H T, Müller T, Böttcher R and Abicht H-P 2003 *Solid State Sci.* **5** 965
[21] Langhammer H T, Müller T, Böttcher R, Mueller V and Abicht H-P 2004 *J. Eur. Ceram. Soc.* **24** 1489
[22] Sawaguchi E, Akishige Y and Kobayashi M 1985 *Japan. J. Appl. Phys.* **24** 252
[23] Akishige Y 1994 *J. Korean Phys. Soc.* **27** S81
[24] Yamaguchi H, Yamada A, Uwe H and Sakudo T 1991 *Phys. Rev.* B **43** 4473
[25] Akishige Y, Yamazaki Y and Mori N 2004 *J. Phys. Soc. Japan* **73** 1267
[26] Yamamoto T, Akishige Y and Sawaguchi E 1988 *J. Phys. Soc. Japan* **57** 3665
[27] Mashkina E, McCammon C and Seifert F 2004 *J. Solid State Chem.* **177** 262
[28] Noda Y, Akiyama K, Shobu T, Kuroiwa Y, Nakao H, Morii Y and Yamaguchi H 1998 *Ferroelectrics* **217** 1
[29] Wang S-F, Hsu Y-C, Chu J P and Wu C-H 2006 *Appl. Phys. Lett.* **88** 042909
[30] Yu J, Itoh M and Saita Y 2005 *Appl. Phys. Lett.* **87** 252904
[31] Rudowicz C 2000 *Crystal Field Handbook* ed D J Newman and B Ng (Cambridge: Cambridge University Press) pp 259–68
[32] Rudowicz C and Jian Q 2002 *Comput. Chem.* **26** 149
[33] Rudowicz C 1987 *Magn. Reson. Rev.* **13** 1
Rudowicz C 1988 *Magn. Reson. Rev.* **13** 335 (erratum)
[34] Rudowicz C 1985 *J. Phys. C: Solid State Phys.* **18** 1415
Rudowicz C 1985 *J. Phys. C: Solid State Phys.* **18** 3837 (erratum)
[35] Rudowicz C and Chung C Y 2004 *J. Phys.: Condens. Matter* **16** 5825
[36] Stevens K W H 1952 *Proc. Phys. Soc.* **65** 209
[37] Newman D J and Urban W 1975 *Adv. Phys.* **24** 793
[38] Rudowicz C 2000 *J. Phys.: Condens. Matter* **12** L417
[39] Rudowicz C 1986 *J. Chem. Phys.* **84** 5045
[40] Rudowicz C and Qin J 2004 *J. Lumin.* **110** 39
[41] Rudowicz C and Sung H W F 2001 *Physica* B **300** 1
[42] Rudowicz C and Misra S K 2001 *Appl. Spectrosc. Rev.* **36** 11
[43] Bacquet G, Dugas J, Escribe C, Gaite J M and Michoulier J 1974 *J. Phys. C: Solid State Phys.* **7** 1551
[44] Rudowicz C and Gnutek P 2008 *Physica* B **403** 2349
[45] Butler P H 1981 *Point Group Symmetry Applications* (New York: Wiley)
[46] Newman D J and Ng B 1989 *Rep. Prog. Phys.* **52** 699
[47] Newman D J and Siegel E 1976 *J. Phys. C: Solid State Phys.* **9** 4287
[48] Glinchuk M D, Bykov I P, Kornienko S M, Laguta V V, Slipenyuk A M, Bilous A G, V'yunov O I and Yanchevskii O Z 2000 *J. Mater. Chem.* **10** 941
[49] Possenriede E, Jacobs P and Schirmer O F 1992 *J. Phys.: Condens. Matter* **4** 4719
[50] Chang Y M, Wang H F and Rudowicz C 1995 *J. Opt. Soc. Am.* B **12** 544
[51] Ebisu H, Arakawa M and Takeuchi H 2005 *J. Phys.: Condens. Matter* **17** 4653
[52] Takeuchi H, Ebisu H and Arakawa M 2008 *J. Phys.: Condens. Matter* **20** 055221
[53] Langhammer H T, Müller T, Böttcher R and Abicht H-P 2008 *J. Phys.: Condens. Matter* **20** 085206